Journal of the Taiwan Institute of Chemical Engineers 145 (2023) 104781

Contents lists available at ScienceDirect

Journal of the Taiwan Institute of Chemical Engineers

journal homepage: www.journals.elsevier.com/journal-of-the-taiwan-institute-of-chemical-engineers

The effect of external force and magnetic field on atomic behavior and pool boiling heat transfer of Fe_3O_4 /ammonia nanofluid: A molecular dynamics simulation

Shouliang Dong [a,*], Hasan Sh. Majdi [b], As'ad Alizadeh [c], Russul Thaibat [d], Furqan S. Hashim [e], Hasan Mohammed Abdullah [f], Qusay Husam Aziz [g], Maboud Hekmatifar [h,*], Rozbeh Sabetvand [i]

[a] School of Chemical Engineering, Qinghai University, Xining, Qinghai 810016, China
[b] Department of Chemical Engineering and Petroleum Industries, Al- Mustaqbal University College, Hilla 51001, Iraq
[c] Department of Civil Engineering, College of Engineering, Cihan University-Erbil, Erbil, Iraq
[d] Medical Lab. Techniques department, College of Medical Technology, Al-Farahidi University, Iraq
[e] Department of Medical Laboratories Technology, AL-Nisour University College, Baghdad, Iraq
[f] Department of Optical Techniques, Al-Zahrawi University College, Karbala, Iraq
[g] Department of Anesthesia Techniques, AlNoor University College, Nineveh, Iraq
[h] Department of Mechanical Engineering, Khomeinishahr Branch, Islamic Azad University, Khomeinishahr, Iran
[i] Department of Energy Engineering and Physics, Faculty of Condensed Matter Physics, Amirkabir University of Technology, Tehran, Iran

ARTICLE INFO

Keywords:
Pool boiling
Ammonia/Fe_3O_4
Nanofluid
Molecular dynamics
External force

ABSTRACT

Background: In this study, the pool boiling heat transfer of Fe_3O_4 /ammonia nanofluid in a copper (Cu) nanochannel is done using the molecular dynamics (MD) simulation.
Methods: To increase and improve the performance of heat transfer, the effect of external force, and external magnetic field frequency on the atomic and thermal performance of the simulated nanostructure was checked. The results show that the density increased with a positive slope when the external force was imposed on the nanostructure with a growing trend. The amount of velocity and temperature similarly increased. So, by increasing the external force from 0.001 to 0.005 eV/Å, the maximum values of density, velocity, and temperature converge to the values of 0.1441 atom/Å^3, 13.939 Å/fs, and 794.61 K. Moreover, increasing the applied external force caused an increase in the heat flux and thermal conductivity in the nanostructure. Finally, studying the effect of external magnetic field on the nanofluid's atomic behavior shows that with the change in the frequency of external magnetic field, Poiseuille behavior was remained. The results of the increase in the frequency of external magnetic field show the increasing trend of velocity and temperature. Numerically, the maximum values of velocity and temperature increase from 7.133 to 11.476 Å/fs, and from 210.23 to 410.07 K, respectively. Furthermore, HF increases by increasing the frequency of external magnetic field.
Significant findings: As particles' movement increased, the structure's thermal resistance decreased. So, by increasing external force, the thermal resistance in the structure decreased.

1. Introduction

At the same time as the climate crisis worsens, the world is investing in carbon-free energy to create a world where either the production of greenhouse gasses is zero or the same amount of greenhouse gas is emitted from the world's blow air [1,2]. There are various methods to reduce using the fossil fuels, such as using green hydrogen [3] or alternative catalyst and fuel refrigerants [4]. Natural gas is one of the world's cleanest fossil fuels. Ammonia is a natural refrigerant compatible with the environment. This refrigerant has excellent thermodynamic and thermal properties. It is widely used in large refrigeration systems. It was used in industries, such as the refrigerators and air conditioners. Studying the biological and environmental effects of refrigerants (synthetic and natural) showed that in the long term, using the natural refrigerants in various refrigeration and air conditioning industries was recommended [5,6]. According to the heat transfer

* Corresponding authors.
E-mail addresses: 2014990009@qhu.edu.cn (S. Dong), Maboud.Hekmatifar@iaukhsh.ac.ir (M. Hekmatifar).

https://doi.org/10.1016/j.jtice.2023.104781
Received 27 December 2022; Received in revised form 28 February 2023; Accepted 1 March 2023
Available online 21 March 2023

characteristics of ammonia, this refrigerant is the most suitable for thermophysical properties [7,8]. Today, the need for effective cooling in small systems was increased in terms of the advances in nanotechnology. The research shows that adding the nanoparticles improved the thermal behavior of different fluids due to having a higher conductivity coefficient than fluids. To be more precise, two main characteristics of nanoparticles are very high stability, and the other is a very high coefficient of thermal conductivity [9–11]. Also, previous studies show that applying a magnetic field can improve the performance of fluid inside the atomic duct [12]. Nanofluids that contain magnetic nanoparticles are widely used in various fields in terms of their higher heat transfer capabilities [13].

Nanofluid heat transfer applications are very important and practical [14,15]. Several studies were conducted in pool boiling heat transfer [16–19]. Whenever the temperature of an object immersed in a liquid, such as the wall of a container, was higher than the saturation temperature of fluid associated with it, the phenomenon of pool boiling was observed [20,21]. The boiling process was characterized by forming steam bubbles separated from the hot surface after successive growth [22]. Bubble growth depended on excess temperature, surface material, thermodynamic properties of the fluid, and surface tension. On the other hand, steam formation and boiling on the surface were effective in the heat transfer [23–25].

For example, Wen et al. [26] checked the thermal performance of pool boiling using Al_2O_3 and TiO_2 nanofluids. They showed a 40% improvement in critical HF. Moreno et al. [27] studied the effects of nanoparticle size on critical HF using Al_2O_3 nanoparticles in the base fluid. Amiri et al. [28] investigated the effect of nanoparticles to improve the critical HF. They used multi-walled carbon nanotubes (MWCNT) with different diameters. They found that the diameter of nanotubes affected the critical HF, and as the diameter of nanotubes increased, the amount of HF decreased. Kim et al. [29] perused the effect of surface moisture on pool boiling heat transfer and critical HF with SiO_2, ZrO_2, and Al_2O_3. The results show that the critical HF increased to 80%, and the heat transfer coefficient was weakly improved. Vitarana et al. [30] perused nanofluids' boiling heat transfer coefficients of Au-H_2O, SiO_2 - H_2O, and SiO_2-ethylene glycol in a cylindrical chamber. This research revealed the improvement of critical HF and heat transfer coefficients between 11% and 21%. Prag et al. [31] investigated the pool boiling using nanofluids based on MWCNTs. Tlili et al. . [32] examined the effect of channel dimensions on the thermal behavior of air in the presence of phase change materials. Dero et al. [33] examined the thermal stability of water/copper-alumina nanofluid.

Due to solving and explaining many phenomena using laboratory methods was impossible or very expensive and time-consuming, today, it is possible to solve many problems using computational methods. For instance, Rajakarunakaran et al. [34] examined the mechanical behavior of self-compacting concrete using numerical methods. The obtained results reveal that it predicts the mechanical behavior of studied structure well. Bai et al. [35] examined the effect of concentration and graphene oxide nanoparticles on the thermal behavior of water/ graphene oxide nanofluid using different numerical methods. The results show that numerical methods could predict the studied structure's thermal performance. Banawas et al. [36] examined the effect of initial temperature and pressure on the thermal and mechanical behavior of calcium phosphate cement using MD simulation. The results show that decreasing the temperature and increasing the pressure led to improving the thermal and mechanical stability of structure. Aljaloud et al. [37] examined the effect of concentration and radius of copper oxide nanoparticles on the thermal behavior of water/copper oxide nanofluid using MD simulation. Different simulation methods and experimental tests were reported to predict pool boiling characteristics in nanofluids. For instance, Liang et al. [38] examined the effect of Fe nanoparticle size on the pool boiling heat transfer using the MD simulation. In another study, Tian et al. [39] examined the effect of external force on the pool boiling of Fe/water nanofluid.

On the other hand, previous studies showed that adding an external magnetic field and electric field can improve heat transfer in a micro/nanochannel. For instance, Wang et al. [40] examined the effect of external electric fields on the nanofluid heat transfer. In a review paper, Wang et al. [41] examined the effect of external magnetic, and electric fields on nanofluid heat transfer. The results show that adding these external field significantly increased the nanofluid heat transfer. Due et al. [42] examined the effect of an external magnetic field on water/Fe_3O_4 nanofluid heat transfer.

Besides, the change in HF, density, temperature, and velocity profile of nanoparticles by increasing the external magnetic and external force were studied. For this purpose, the frequency of external magnetic field with different values of 0.01, 0.02, 0.03, and 0.05 1/ps, and the external force with values of 0.001, 0.002, 0.003, and 0.005 eV/Å were applied to nanofluid.

2. The MD simulation formulation

The main benefit of computer simulations help understand the properties of molecules in terms of structure and their microscopic interactions. The MD is a simulation method that helps us investigate the system's dynamical properties [43]. The MD simulation predicts the movements and trajectories of interacting particles over time. This aim was fulfilled by numerical solving the classical Newton's equation of motion [44]. The numerical solving of Newton's equation was performed using a method called velocity-Verlet integration. The velocity-Verlet algorithm calculated the velocity and the position of a particle in a time step Δt [44].

The thermal conductivity and HF of simulated structures were calculated from the Green-Kubo formulation.The Green-Kubo formula is relates the ensemble average of the auto-correlation of the HF to kappa. The HF can be calculated from the fluctuations of per-atom potential and kinetic energies and per-atom stress tensor in a steady-state equilibrated simulation [45]. Technically, we used 'Compute heat/flux' command in the LAMMPS package witch can calculate the needed HF and describes how to implement the Green_Kubo formalism [45]. These formulisem are represented as follows (Eqs. (1) and (2)) [46–48]:

$$K = \frac{V}{K_B T^2}\int_0^\infty \langle J_x(0)J_x(t)\rangle dt = \frac{V}{3K_B T^2}\int_0^\infty \langle \mathrm{J}(0).\mathrm{J}(t)\rangle dt \tag{1}$$

where, J indicates HF, V indicates the volume, T shows the temperature, and K_B represents the Boltzmann constant ($1.380649 \times 10^{-23}\ m^2.kg.s^{-2}.K^{-1}$). In the case of two-body interactions, the HF **J** is defined as:

$$\begin{aligned} \mathrm{J} &= \frac{1}{V}\left[\sum_i e_i \mathrm{v}_i - \sum_i \mathrm{S}_i \mathrm{v}_i\right] \\ &= \frac{1}{V}\left[\sum_i e_i \mathrm{v}_i - \sum_{i<j}\left(\mathrm{F}_{ij}.\mathrm{v}_j\right)\mathrm{r}_{ij}\right] \\ &= \frac{1}{V}\left[\sum_i e_i \mathrm{v}_i - \frac{1}{2}\sum_{i<j}\left(\mathrm{F}_{ij}.\left(\mathrm{v}_i+\mathrm{v}_j\right)\mathrm{r}_{ij}\right]\right. \end{aligned} \tag{2}$$

where, e_i shows the per-atom energy (potential and kinetic), S_i represents the per-atom stress tensor, v_i represents the particle velocity, F_{ij} is the force exerted on the i and j particles, and V indicates the volume.

The atomic structures simulated in the upcoming research had a defined electric charge from a computational point of view. When the pregnant particle moved in the magnetic field, it always experienced a force that was perpendicular to the field. As a result, greater mobility and velocity will be visible in these samples in the nanochannel. The external magnetic fields were used to atomic samples by following formulations:

$$B = B_0 sin(\omega t) \tag{3}$$

In this equation, B_0 is the amplitude of external magnetic field (0.1 T), and ω is the frequency of this external factor. To study the effect of this external factor on the simulated samples' atomic performance, the external fields' frequencies were 0.01,0.02, 0.03, and 0.05 ps^{-1}.

The most important part of each simulation was to examine the interactions among particles, which were defined via the potential function. Previous studies show that the Lennard-Jones potential function was suitable for modeling ammonia structure. Furthermore, the metallic structure of nanoparticles was used from the EAM potential function [49,50]. This simulation used EAM, Lennard-Jones (LJ), and Columb potential. EAM potential function definition:

$$U_i = F_\alpha\left(\sum_{i\neq j}\rho_\beta(r_{ij})\right) + \frac{1}{2}\sum_{i\neq j}\phi_{\alpha\beta}(r_{ij}) \tag{4}$$

where, F_α, $\varphi_{\alpha\beta}$, ρ_β, and r_{ij} in above equation were the acts as the function of electron density, a pair potential interaction, absorbent force, and the distance among particles, respectively. Alpha (α) and beta (β) are the element types of atoms I and J. LJ potential function is defined as follows [51]:

$$U_{LJ} = 4\varepsilon_{ij}\left[\left(\frac{\sigma_{ij}}{r_{ij}}\right)^{12} - \left(\frac{\sigma_{ij}}{r_{ij}}\right)^{6}\right] r_{ij} < r_c \tag{5}$$

where, σ_{ij} and ε_{ij} are the depth of particle potential well, the finite distance in the case the potential was zero. The r_{ij} shows the distance among the particles, and indices i and j represent the element types of atoms I and J. And r_c represents the cutoff radius (12 Å). LJ potential parameters for each present particle in the MD simulation in terms of selective force field are presented in Table 1. These coefficients are written from the UFF and DREIDING references [52,53].

Due to Table 1, σ_{ij} and ε_{ij} of each particles are calculated using Eqs. (6) and (7) [54]:

$$\varepsilon_{ij} = \sqrt{\varepsilon_i \varepsilon_j} \tag{6}$$

$$\sigma_{ij} = \frac{\sigma_i + \sigma_j}{2} \tag{7}$$

Furthermore, the electric potential energy is described by Coulombic interactions (8) [55]:

$$U_{ij} = \frac{C q_i q_j}{\varepsilon r_{ij}} r_{ij} < r_c \tag{8}$$

where, C is an energy-conversion constant, q_i and q_j are the charges on the 2 atoms, and ε is the dielectric constant. The cutoff r_c truncates the interaction distance

2.1. The MD simulation process in current research

This research studied pool boiling heat transfer of ammonia nanofluid containing Fe_3O_4 nanoparticles in a nanochannel using LAMMPS software. A simulation box with the dimension of 100 × 60 × 60 $Å^3$ was considered in the present simulation. A nanochannel with a thickness of 5 Å was modeled, along with the length of simulation box. This simulated nanochannel is made of Cu particles. One sphere of Fe_3O_4 nanoparticles with a radius of 10 Å was modeled. An example of modeled structure that included nanochannel and nanofluid is represented in Figs. 1 and 2. The initial temperature was set to 195 K using the NVT ensemble. The current simulation consisted of two basic parts. In the first part, using the NVT ensemble, the desired nanostructure reached equilibrium at a temperature of 195 K. To check the equilibration in the structure, the changes in potential energy and total energy were checked (In Supporting Information section). The convergence of these quantities to a constant number showed the equilibrium in the simulated structure. Moreover, the convergence in the mentioned quantities was in terms of appropriate force field. The Nose-Hoover thermostat was used to check the equilibrium in temperature.

Table 1
The LJ parameters in the present MD simulation [52,53].

Type of Particles	σ_i (Å)	ε_i (kcal/mol)
Cu	3.495	0.005
H	2.886	0.044
O	3.5	0.06
Fe	4.54	0.055
N	3.995	0.415

3. Result and discussion

3.1. Effects of magnetic field frequency on the atomic and thermal performance of nanostructure

Under the effect of external magnetic field, it had an increasing or decreasing trend. Consequently, it is expected that the boiling of this material in terms of the magnetic field will include various results and phenomena. It will be possible to change the applied external magnetic field in the studied samples via a change in the field amplitude and a change in the frequency of this field. Therefore, the parameters, such as temperature, density, and velocity profile, which were affected by the magnetic field with different frequencies and illustrate various behavior, were analyzed in the current research.

The values of these quantities were measured, and finally averaged in each bin. Finally, the averaged thermophysical parameters were plotted based on the properties of various bins. Therefore, the density profile of studied nanofluid was drawn based on the density of particles in each bin as shown in Fig. 3. The 'compute chunk/atom' command was used to calculate the density profile. This compute examined the number of atoms in each bin volume [56]. As a result, the interactions between the nanochannel walls and the nanofluid particles dominated. Since the studied structure's particle number did not change, it is expected that the density of nanofluid will not change while the external field's frequency changes.

Fig. 4 shows the velocity profiles in the desired nanostructure versus increasing the frequency of the external magnetic field. The increase in atomic oscillations in the ammonia-Cu nanofluid was created in terms of the increase in frequency. Therefore, the arrangement of velocity profile and the maximum numerical value of this quantity changed. Quantitative results represent that the maximum velocity of particles was equal to 11.476 Å/fs, which was obtained using the frequency with a magnitude of 0.05 1/ps.

On the other hand, an increase in the amount of movement and mobility of nanoparticles was obtained by increasing the frequency, which will lead to changes in the temperature of atomic structures, according to Fig. 5. Fig. 5 shows the temperature profile changes in the nanochannel versus increasing the frequency of magnetic field. By the change in the atomic behavior of studied nanostructure, it is expected that this behavior had a direct effect on the thermal behavior of these nanostructures, so these cases and changes should be considered in the field of the practical application of these atomic samples. The numerical results obtained from this part are fully presented in Table 2.

As mentioned earlier, positive changes in the magnetic field frequency caused the improvement of the oscillatory behavior and the amount of mobility of nanostructures. Therefore, studying the thermal behavior of this nanostructure under new conditions will be important. Fig. 6 shows the changes in the amount of HF flowing in the nanochannel versus the increased frequency of magnetic field. In this part, the HF variations are examined in terms of ΔT, where the T variations are equal to:

$$\Delta T = T_s - T_{sat} \tag{9}$$

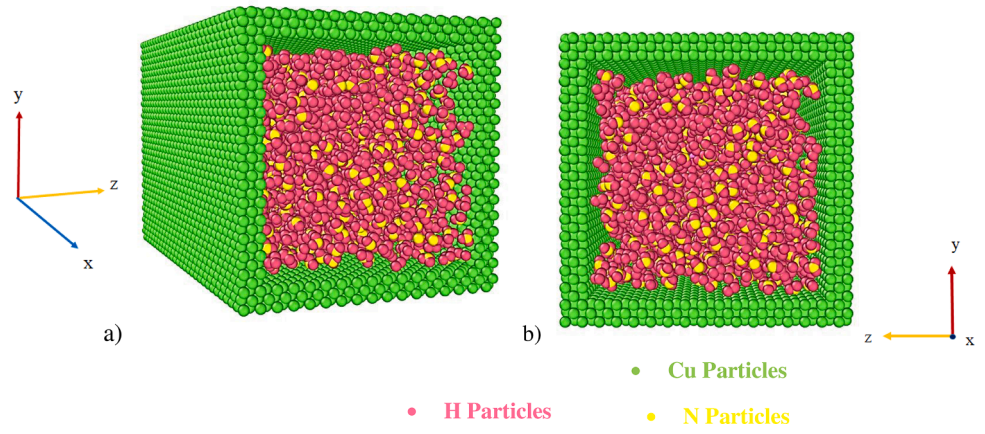

Fig. 1. General representation of the desired nanostructure from a) perspective and b) front view.

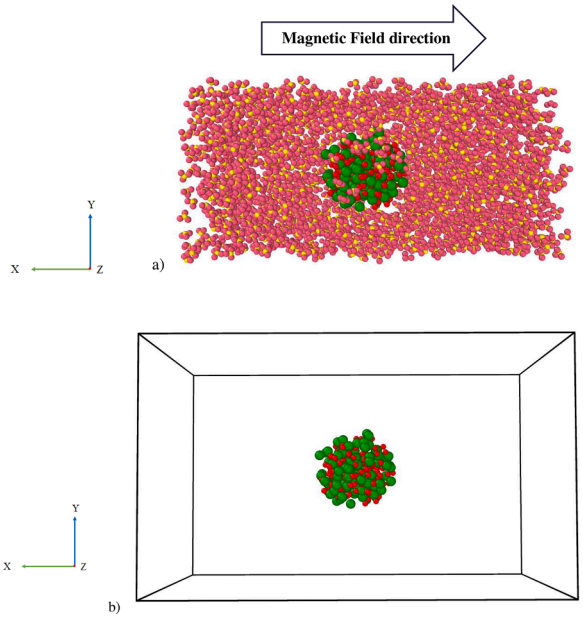

Fig. 2. A schematic of a) ammonia/ Fe_3O_4 nanofluid and b) Fe_3O_4 nanoparticle in the present simulation.

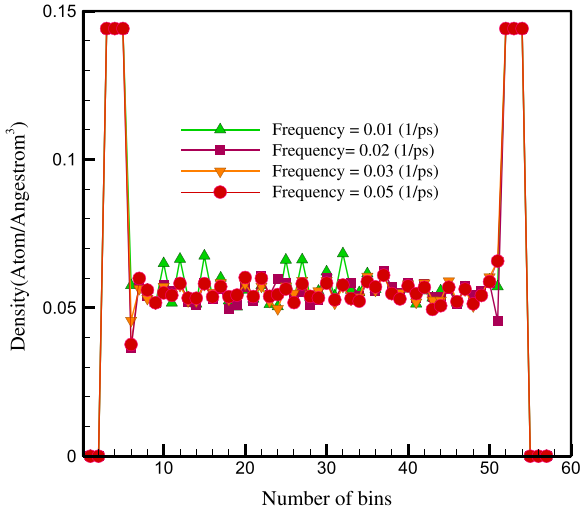

Fig. 3. Changes in nanofluid density profile vs. increasing magnetic field frequency.

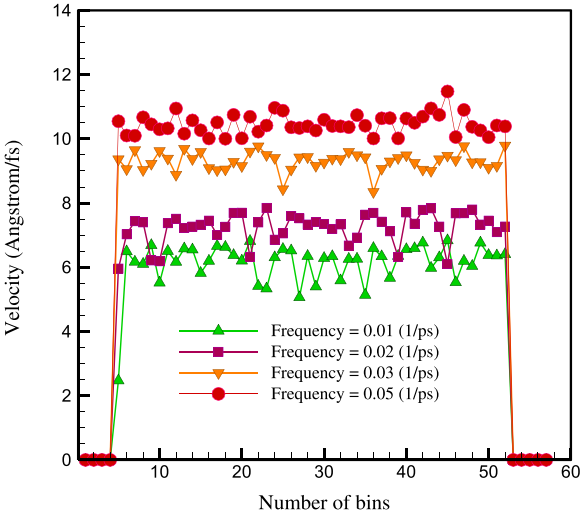

Fig. 4. Changes in nanofluid velocity profile vs. increasing magnetic field frequency.

where, T_{sat} and T_s are the saturation T and surface T. As it is well known, the HF diagram exhibits an increase-decrease-increase pattern under the specified conditions, indicating the sample's poolboiling hear transfer procedure. Based on the results presented in Fig. 6, increasing the frequency of external magnetic field led to an increase in the HF transferred in the nanochannel.

As the temperature increased, these bubbles joined together and reduced the heat transfer (more details in Section 5.2 (Boiling Curve)). As the bubbles' size increased, the fluid's density decreased [57]. Fig. 7 shows the density profile changes before and after the critical heat flux in the presence of a magnetic field with 0.01 1/ps frequency magnitude. Numerically, the maximum density of particles was equal to 0.1405 and 0.1277 atom/$Å^3$ before and after the critical heat flux. This decrease in density was in terms of the formation of bubbles on the surface of fluid.

In the discussion of time series, there was a dependence among the observations based on time. Since in statistics, dependence is often expressed as correlation, and the word autocorrelation means serial correlation or dependence among the sequential values in terms of time. Fig. 8 represents the change in heat flow autocorrelation function (HFAF) of the simulated structure over the timestep. This chart was

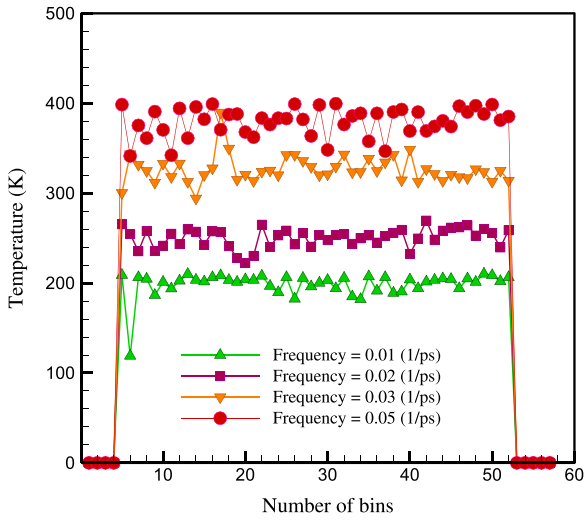

Fig. 5. Changes in nanofluid temperature profile vs. increasing frequency.

Table 2
The maximum values of density, velocity, and temperature vs. the applied external magnetic field frequency.

Frequency of magnetic field (1/ps)	Maximum density (atom/Å^3)	Maximum velocity (Å/fs)	Maximum temperature (K)
0.01	0.1441	7.133	210.23
0.02	0.1442	7.8492	279.69
0.03	0.1441	9.795	339.81
0.05	0.1444	11.476	410.07

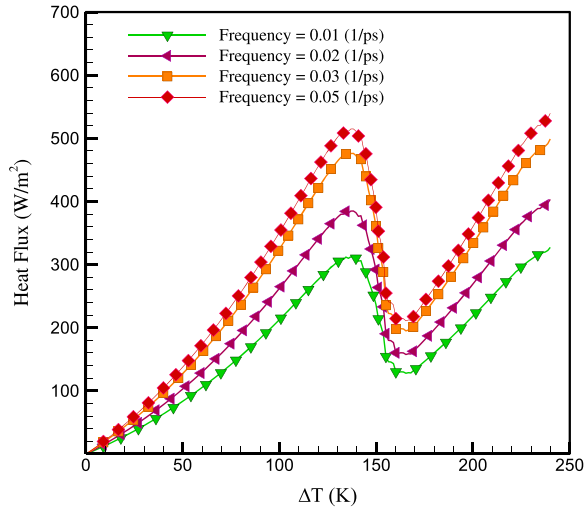

Fig. 6. Changes in HF vs. the excess temperature difference for different values of the frequency of the external magnetic field.

descending in order of delay. The longer the observations were delayed, the less correlation they found. Fig. 8 show that the HFAF condensation of the simulated structure converged to zero with oscillating performance. Following Green-Kubo equation, the HFAF convergence to zero showed thermal conductivity convergence [58].

Fig. 9 and Table 3 show the changes in thermal conductivity with the increased frequency of magnetic field. The previous studies showed that by increasing the magnetic field magnitude, the thermal conductivity showed an upward behavior [59–61]. This increase was due to the increase in the velocity and movement of the particles with the increase in

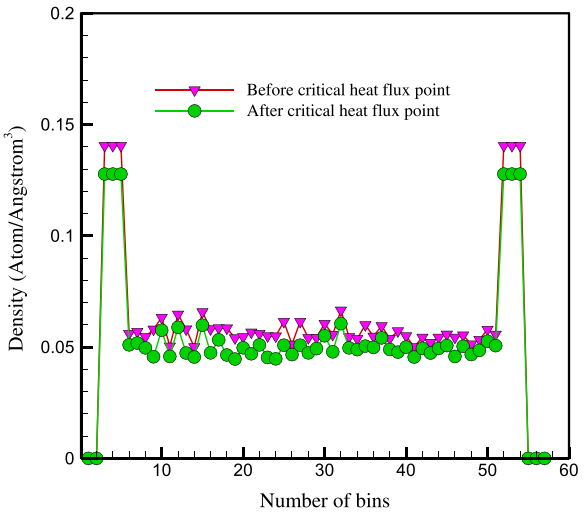

Fig. 7. Changes in nanofluid density profile before and after the critical heat flux in the presence of a magnetic field with 0.01 1/ps frequency magnitude.

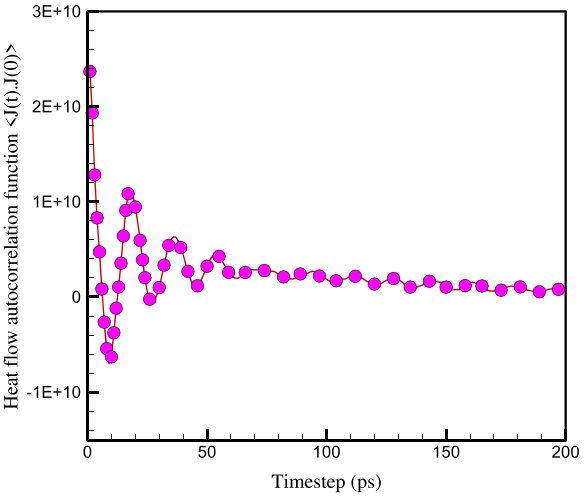

Fig. 8. The change in HFAF of simulated structure over the timestep.

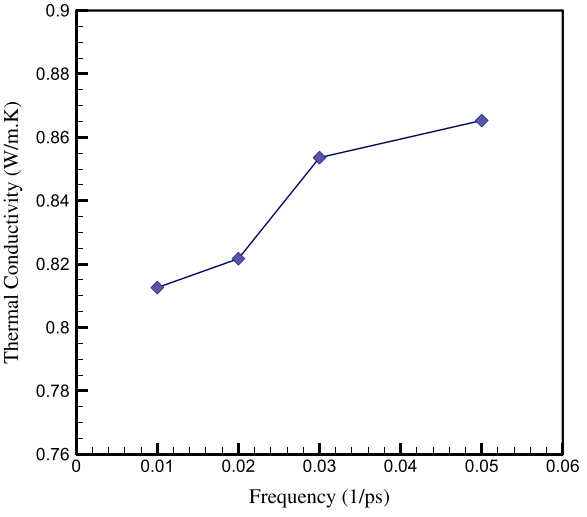

Fig. 9. Changes in thermal conductivity vs. frequency of the external magnetic field.

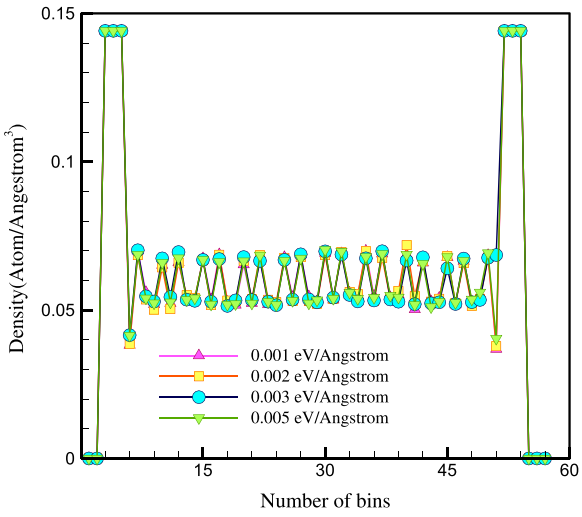

Fig. 10. Changes in density profile vs. increasing external force.

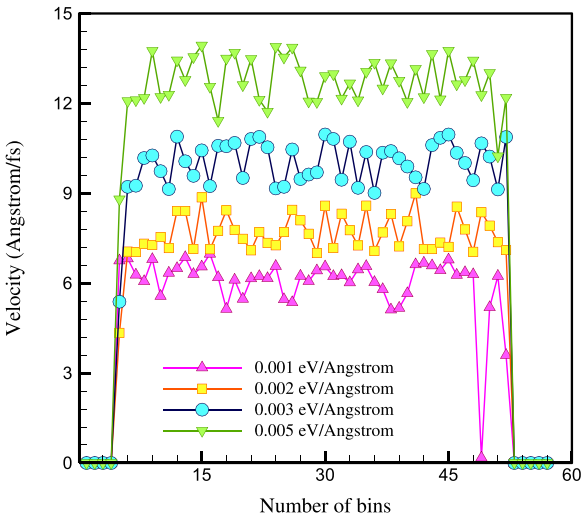

Fig. 11. Changes in nanofluid velocity profile vs. increasing external force.

Table 3
Changes in thermal conductivity of simulated nanofluid vs. frequency of the external magnetic field.

Frequency of magnetic field	0.01 (1/ps)	0.02 (1/ps)	0.03 (1/ps)	0.05 (1/ps)
Thermal Conductivity	0.813 (W/m.K)	0.821 (W/m.K)	0.854 (W/m.K)	0.866 (W/m.K)

the magnitude of magnetic field. Generally, applying a magnetic field leads to a change in the direction of the particles in the magnetic nanofluid. This change in direction leads to an increase in the energy and acceleration of the particles. So, the magnetic field itself does not change the velocity of the particles [62].The higher the velocity of the particles, the more they collide, so heat transfer occurred at a higher rate. In general, as the frequency increased, the energy of the particles increased. Energy determines the reaction rate factor. Therefore, by increasing energy, the velocity and movement of particles improved. Moreover, the temperature of particles increased [63]. Therefore, it can be said that the with increasing the magnetic field magnitude, the particles are accelerated [64]. As more charge is put in more motion, the better the thermal behavior of the magnetic nanofluid [65]. Previous studies reported thermal conductivity for ammonia fluid in the range from 0.7 to 0.8 W/m.K [66].

3.2. The effect of external force on the atomic and thermal behavior of nanostructure

The external force applied from the surrounding environment to desired nanostructure is an important and influential factor. Therefore, to check this factor in this section, different amounts of external force with values of 0.001, 0.002, 0.003, and 0.005 eV/Å were used to the nanostructure as shown in Fig. 10. Considering in this simulation, the composition of studied nanostructures didn't change due to the atomic ratio of Fe_3O_4 nanoparticles to ammonia fluid particles, the density value in these nanostructures did not change significantly. This change is due to the increase of disturbances related to the bubbles created on the surface of the fluid by increasing the external force. The lack of density change is due to the constant atomic ratio of Fe_3O_4 nanoparticles to ammonia fluid particles, so the density value does not change much in these atomic nanostructures.

Fig. 11 illustrates the fluctuations in the velocity according to the increase of external force applied to the nanofluid. Studying the velocity profile is very important to survey the thermal performance of desired nanostructures. As shown in Fig. 11, the velocity values increase with the external pressure applied to the nanofluid. Numerically, with the increase of external force to 0.005 eV/Å, the velocity of particles reached from 6.977 Å/fs to 13.939 Å/fs. Increasing the external force in the simulated atomic structure increased the mobility of the particles in the nanochannel increases. As a result, the maximum velocity in the nanofluid particles increases. Thus, it can be found that the thermal performance of nanofluids is improved due to such changes.

Fig. 12 shows the changes in the temperature of nanofluid according to the increase of the external force. Numerically, with the increase of external force, the maximum temperature value increased from 398.42 K to 794.61 K. An increase in the pressure applied to the nanostructure was obtained as a result of an increase in the external force. The results of this part are presented in Table 4.

The progress of the thermal performance with the increased external force had a direct relationship with the HF in desired nanostructures. HF in the nanostructure is reported in Fig. 13. Besides, when the external force increased, the pressure on the nanofluid increased. It causes the velocity of nanofluid particles to increase, and HF was transferred with greater intensity and quantity.

Fig. 14 and Table 5 show the changes in thermal conductivity with the increase in external force. By increasing this thermodynamic quantity, it is expected that the heat transfer in the atomic structure will

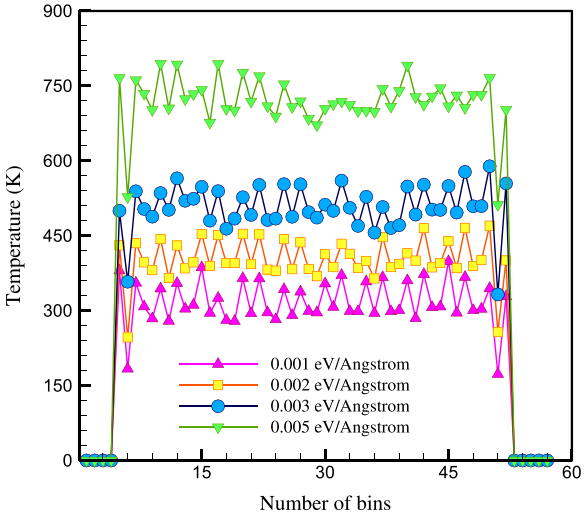

Fig. 12. Changes in nanofluid temperature profile vs. increasing external force.

Table 4
The maximum values of density, velocity, and temperature vs. the applied external force.

External force (eV/Å)	Maximum density (atom/Å^3)	Maximum velocity (Å/fs)	Maximum Temperature (K)
0.001	0.1441	6.997	398.42
0.002	0.1442	8.961	470.36
0.003	0.1441	10.961	589.19
0.005	0.1441	13.939	794.61

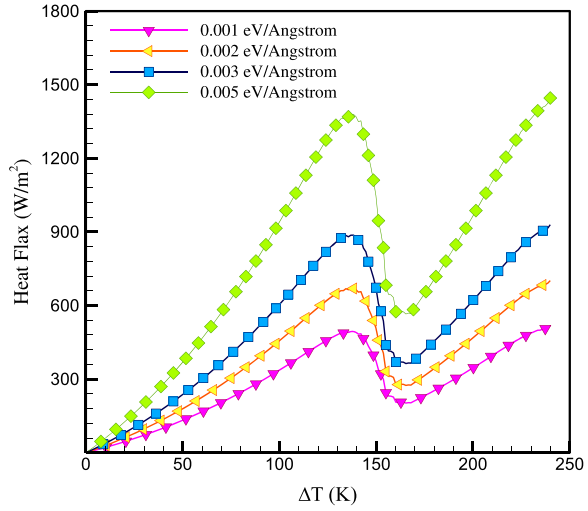

Fig. 13. Changes in HF vs. the excess temperature difference for different values of the external force.

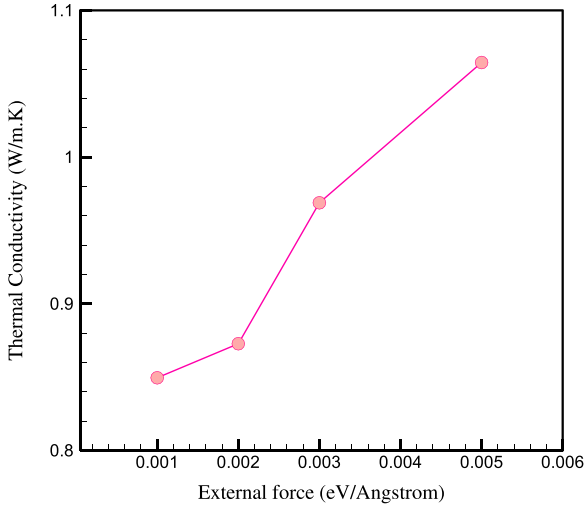

Fig. 14. Changes in thermal conductivity vs. external force.

Table 5
Changes in thermal conductivity of simulated nanofluid vs. external field.

External force	0.001 (eV/Å)	0.002 (eV/Å)	0.003 (eV/Å)	0.005 (eV/Å)
Thermal Conductivity	0.850 (W/m.K)	0.873 (W/m.K)	0.969 (W/m.K)	1.06 (W/m.K)

increase. Finally, the thermal conductivity will increase in the studied samples. Therefore, the structure's thermal resistance decreased with the external force increase.

The obtained results show that adding the external force had a better thermal performance than the magnetic field in the studied structure. Therefore, to improve the thermal performance of studied structure in various industries, an external force can be applied in addition to applying a magnetic field.

4. Conclusion

The current paper analysed the pool boiling process in ammonia-based nanofluid using the MD simulation and LAMMPS software. The ammonia/Fe_3O_4 nanofluid pool boiling process was carried out in a Cu nanochannel. In general, the processes carried out in this research were checked in the two-step, including the equilibration and the investigation of atomic structures' atomic and thermal behavior. In the first step, the equilibrium in the nanostructure was checked. The results showed that:

- The potential energy in the desired nanostructure converged to a −22,451.3 eV after 20 ns passed.
- The amount of total energy in desired nanostructure, which is the sum of the kinetic and potential energies of the nanostructure, converged to a −22,532.3 eV.

In the second step, parameters, such as temperature, velocity, density, and HF of nanostructure were evaluated. The results indicated that:

- Increasing the frequency of external magnetic field from 0.01 1/ps to 0.05 1/ps led to the convergence of velocity and temperature profiles to the numerical values 11.476 Å/fs and 410.07 K.
- The results show that with the increase in the magnetic field frequency (from 0.01 to 0.05 ps^{-1}), the thermal conductivity in the nanofluid increased from 0.813 to 0.866 W/m.K .Consequently, the thermal resistance in the structure decreased. HF increased with increaseng in the external field frequency.
- Increasing the external force to 0.005 eV/Å led to the velocity and temperature profiles increase to 13.939 Å/fs and 794.61 K.
- The results show that an increase in external force led to an increase in HF. By increasing the external force from 0.001 to 0.005 eV/Å, thermal conductivity in the nanofluid increased from 0.850 to 1.06 W/m.K.

5. Supporting information

5.1. Equilibrium process

The simulated sample's equilibration time equals 20 ns. Fig. 15 shows the potential energy changes for nanofluid in 20 ns. The results

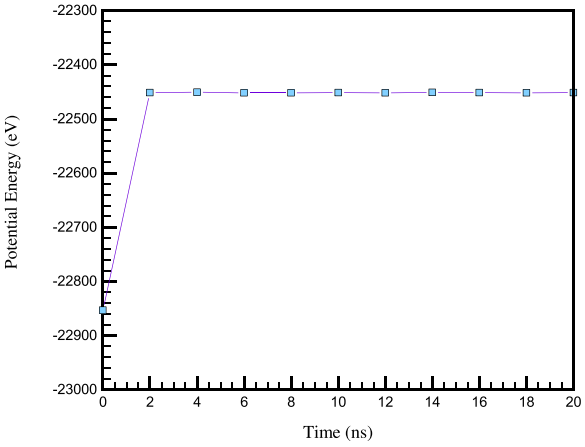

Fig. 15. Potential energy versus time in the presence of nanofluid.

obtained for the potential energy of the desired nanostructure reveal that after 20 ns, this quantity's value approaches negative values. This convergence to a constant value showed sufficient simulation time for the equilibration process. Numerically, the potential energy converged to a value of −22,451.3 eV. The negative value of the potential function showed that the simulated nanostructure had good stability and the attraction force prevails among the existing particles. Convergence in the potential energy of the simulated structure was in terms of appropriate force field. The more negative the potential energy, the more stable the simulated structure.

One of the other important cases studied to determine the behavior of the nanostructure is the total energy. The mentioned quantity accurately predicts the atomic behavior of nanostructure in the subsequent times of simulation. Fig. 16 shows the changes in the total energy for nanofluid after 20 ns. According to the results in Fig. 16, the total energy value in the simulated metal nanochannel with the presence of base fluid approached the numerical value of −22,532.3 eV.

5.2. Boiling curve

Nukiyama studied different areas of pool boiling using a nickel-chrome wire placed in a water reservoir [67]. The heat flux from the nickel-chrome wire to the saturated water was determined by measuring the current intensity and the potential difference. The temperature of wire was obtained from the property of its electrical resistance changes with temperature. According to the diagram below (see Fig. 17), pool boiling had four different regimes.

- **Free Convection Boiling**

Hence, bubbles are not produced, and the free movement mechanism mostly does heat transfer.

- **Nucleate Boiling**

Separate bubbles were formed in this area. By increasing the temperature in this area, the bubbles joined together, and considering the liquid was heated, the bubbles can reach the free surface of the liquid and not be distilled in the liquid. This heat flux is called critical heat flux.

- **Transition boiling**

As the temperature increased further, bubbles accumulated around the joint surface. These bubbles coalesce and reduce heat transfer. Because bubbles contain gas, which had a much lower conductivity than liquid, there will be the lowest heat flux in this temperature difference. This point is called Leidenfrost Point

- **Film Boiling**

The bubble coalition will be eventually broken, large vapor bubbles will be pulled from the surface, and the heat flux will increase by increasing temperature.

6. Future outline

In future studies, multi-particle collision dynamics (MPCD) or MPCD-MD hybrid method methods can be used to study better the process of particle movement, and thermal conductivity of nanofluid. The hybrid method of MPCD-MD will be used to study the effect of aggregation morphology on the thermal conductivity of different nanofluids [69,70]. Therefore, to validate and study more precisely the studied particles' behavior, this hybrid method can be used.

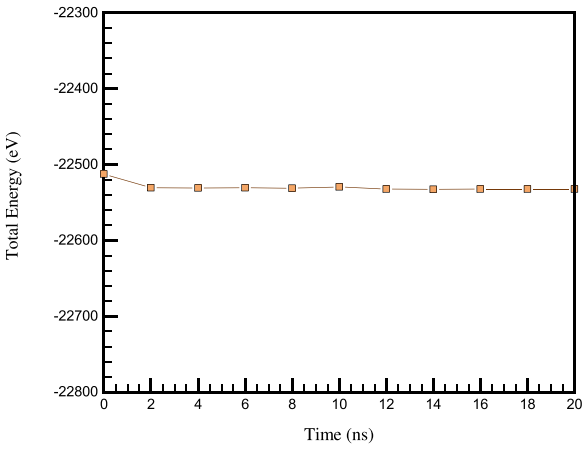

Fig. 16. Total energy versus time in the presence of nanofluid.

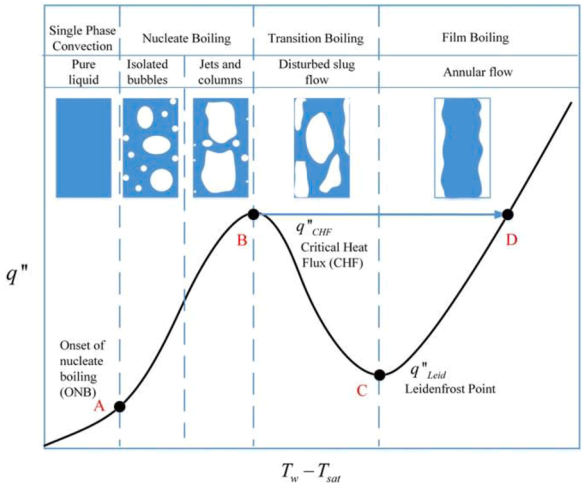

Fig. 17. The Nukiyama curve of pool boiling heat transfer [68].

Declaration of Competing Interest

The authors declare that they have no known competing financial interests or personal relationships that could have appeared to influence the work reported in this paper.

Acknowledgments

1. Exploratory work of plateau (Qinghai) energy efficiency testing laboratory.
2. Special Equipment Inspection Institute of Qinghai Province

References

[1] Akrami E, Khalilarya S, Rocco MV. Techno-economic evaluation of a novel bio-energy system integrated with carbon capture and utilization technology in greenhouses. J Taiwan Inst Chem Eng 2023:104729.
[2] Gao P, Wang Z, Liu L, Cheng S, Li G. Efficient CF4 adsorption on porous carbon derived from polyaniline. J Taiwan Inst Chem Eng 2023;143:104654.
[3] Okonkwo PC, Belgacem IB, Zghaibeh M, Tlili I. Optimal sizing of photovoltaic systems based green hydrogen refueling stations case study Oman. Int J Hydrog Energy 2022;47(75):31964–73.
[4] Wei X, Yang H, Liu B, Yu H, Wang C, Wu S, Jia Z, Han W. Synthesis of titanium oxyfluoride with oxygen vacancy as novel catalysts for pyrolysis of fluorinated greenhouse gasses to hydrofluoroolefins. J Taiwan Inst Chem Eng 2021;129:189–96.
[5] Bolaji B, Huan Z. Ozone depletion and global warming: case for the use of natural refrigerant–a review. Renewable Sustainable Energy Rev 2013;18:49–54.

[6] Ohadi M, Li S, Radermacher R, Dessiatoun S. Critical review of available correlations for two-phase flow heat transfer of ammonia. Int J Refrig 1996;19(4):272–84.
[7] Lorentzen G. Ammonia: an excellent alternative. Int J Refrig 1988;11(4):248–52.
[8] Zhang R, Liu J, Zhang L. Flow boiling heat transfer and dryout characteristics of ammonia in a horizontal smooth mini-tube. Int J Therm Sci 2022;171:107224.
[9] Ilyas SU, Pendyala R, Marneni N. Stability of nanofluids," engineering applications of nanotechnology. Springer; 2017. p. 1–31.
[10] Fuskele V, Sarviya R. Recent developments in nanoparticles synthesis, preparation and stability of nanofluids. Mater Today: Proc 2017;4(2):4049–60.
[11] Hwang Y-j, Lee J, Lee C, Jung Y, Cheong S, Lee C, Ku B, Jang S. Stability and thermal conductivity characteristics of nanofluids. Thermochim Acta 2007;455(1–2):70–4.
[12] Prasad KV, Vaidya H, Oudina FM, Ramadan KM, Khan MI, Choudhari R, Gulab RK, Tlili I, Guedri K, Galal AM. Peristaltic activity in blood flow of Casson nanoliquid with irreversibility aspects in vertical non-uniform channel. J Indian Chem Soc 2022;99(8):100617.
[13] Şeşen M, Tekşen Y, Şendur K, Pınar Mengüç M, Öztürk H, Yağcı Acar H, Koşar A. Heat transfer enhancement with actuation of magnetic nanoparticles suspended in a base fluid. J Appl Phys 2012;112(6):064320.
[14] Yao Z, Derikvand M, Solari MS, Zhang J, Altalbawy FM, Al-Khafaji AHD, Akbari OA, Toghraie D, Mohammed IM. Numerical assessment of the impacts of non-Newtonian nanofluid and hydrophobic surfaces on conjugate heat transfer and irreversibility in a silicon microchannel heat-sink. J Taiwan Inst Chem Eng 2023;142:104642.
[15] Fu X, Abd El-Rahman M, Abdalla AN, Malekshah EH, Sharifpur M. The numerical analysis and optimization of a Photovoltaic thermal collector with three different plain, ribbed, and porous-ribbed absorber tubes and a nanofluid coolant using two-phase model. J Taiwan Inst Chem Eng 2023:104725.
[16] Berenson P. Experiments on pool-boiling heat transfer. Int J Heat Mass Transf 1962;5(10):985–99.
[17] You S, Kim J, Kim K. Effect of nanoparticles on critical heat flux of water in pool boiling heat transfer. Appl Phys Lett 2003;83(16):3374–6.
[18] Vassallo P, Kumar R, D'Amico S. Pool boiling heat transfer experiments in silica–water nano-fluids. Int J Heat Mass Transf 2004;47(2):407–11.
[19] Trisaksri V, Wongwises S. Nucleate pool boiling heat transfer of TiO2–R141b nanofluids. Int J Heat Mass Transf 2009;52(5–6):1582–8.
[20] Hinds D, Maslak C. Next-generation nuclear energy: the ESBWR. Nuclear News 2006;49(1):35–40.
[21] Pioro I, Rohsenow W, Doerffer S. Nucleate pool-boiling heat transfer. I: review of parametric effects of boiling surface. Int J Heat Mass Transf 2004;47(23):5033–44.
[22] Huang M, Yang Z, Duan Y-Y, Lee D-J. Bubble growth for boiling bubbly flow for R141b in a serpentine tube. J Taiwan Inst Chem Eng 2011;42(5):727–34.
[23] Bergles AE. Enhancement of pool boiling. Int J Refrig 1997;20(8):545–51.
[24] Han C-Y. The mechanism of heat transfer in nucleate pool boiling. Massachusetts Inst Technol 1962.
[25] Ahn HS, Sathyamurthi V, Banerjee D. Pool boiling experiments on a nano-structured surface. IEEE Trans Compon Packag Technol 2009;32(1):156–65.
[26] Wen D, Ding Y. Experimental investigation into the pool boiling heat transfer of aqueous based γ-alumina nanofluids. J Nanopart Res 2005;7(2):265–74.
[27] Moreno Jr G., Oldenburg S.J., You S.M., and Kim J.H. Pool boiling heat transfer of alumina-water, zinc oxide-water and alumina-water+ ethylene glycol nanofluids. 2005; 625–632.
[28] Amiri A, Shanbedi M, Amiri H, Heris SZ, Kazi SN, Chew BT, Eshghi H. Pool boiling heat transfer of CNT/water nanofluids. Appl Therm Eng 2014;71(1):450–9.
[29] Kim HD, Kim J, Kim MH. Experimental studies on CHF characteristics of nano-fluids at pool boiling. Int J Multiphase Flow 2007;33(7):691–706.
[30] Witharana S. Boiling of refrigerants on enhanced surfaces and boiling of nanofluids. Energiteknik 2003.
[31] Thakur P, Kumar N, Sonawane SS. Enhancement of pool boiling performance using MWCNT based nanofluids: a sustainable method for the wastewater and incinerator heat recovery. Sustain Energy Technol Assess 2021;45:101115.
[32] Tlili I, Alharbi T. Investigation into the effect of changing the size of the air quality and stream to the trombe wall for two different arrangements of rectangular blocks of phase change material in this wall. J Build Eng 2022;52:104328.
[33] Dero S, Abdelhameed T, Al-Khaled K, Lund LA, Khan SU, Tlili I. Contribution of suction phenomenon and thermal slip effects for radiated hybrid nanoparticles (Al2O3-Cu/H2O) with stability framework. Int J Mod Phys B 2022:2350147.
[34] Rajakarunakaran SA, Lourdu AR, Muthusamy S, Panchal H, Alrubaie AJ, Jaber MM, Ali MH, Tlili I, Maseleno A, Majdi A. Prediction of strength and analysis in self-compacting concrete using machine learning based regression techniques. Adv Eng Softw 2022;173:103267.
[35] Bai J, Kadir DH, Fagiry MA, Tlili I. Numerical analysis and two-phase modeling of water graphene oxide nanofluid flow in the riser condensing tubes of the solar collector heat exchanger. Sustain Energy Technol Assess 2022;53:102408.
[36] Banawas S, Ibrahim TK, Tlili I, Le QH. Reinforced Calcium phosphate cements with zinc by changes in initial properties: a molecular dynamics simulation. Eng Anal Bound Elem 2023;147:11–21.
[37] Aljaloud ASM, Smida K, Ameen HFM, Albedah M, Tlili I. Investigation of phase change and heat transfer in water/copper oxide nanofluid enclosed in a cylindrical tank with porous medium: a molecular dynamics approach. Eng Anal Bound Elem 2023;146:284–91.
[38] Liang Q, Valizadeh K, Bateni A, Patra I, Abdul-Fattah MN, Kandeel M, Zahra MMA, Bashar BS, Baghaei S, Esmaeili S. The effect of type and size of nanoparticles and porosity on the pool boiling heat transfer of water/Fe nanofluid: molecular dynamics approach. J Taiwan Inst Chem Eng 2022;136:104409.
[39] Tian Y, Patra I, Majdi HS, Ahmad N, Sivaraman R, Smaisim GF, Hadrawi SK, Alizadeh Aa, Hekmatifar M. Investigation of atomic behavior and pool boiling heat transfer of water/Fe nanofluid under different external heat fluxes and forces: a molecular dynamics approach. Case Stud Therm Eng 2022;38:102308.
[40] Wang R, Chen T, Qi J, Du J, Pan G, Huang L. Investigation on the heat transfer enhancement by nanofluid under electric field considering electrophorestic and thermophoretic effect. Case Stud Therm Eng 2021;28:101498.
[41] Wang G, Zhang Z, Wang R, Zhu Z. A review on heat transfer of nanofluids by applied electric field or magnetic field. Nanomaterials 2020;10(12):2386.
[42] Du J, Wang R, Zhuo Q, Yuan W. Heat transfer enhancement of Fe3O4-water nanofluid by the thermo-magnetic convection and thermophorestic effect. Int J Energy Res 2022;46(7):9521–32.
[43] Allen MP. Introduction to molecular dynamics simulation. Computat Soft Matter: Synth Polym Proteins 2004;23(1):1–28.
[44] Rapaport DC, Rapaport DCR. The art of molecular dynamics simulation. Cambridge university press; 2004.
[45] https://docs.lammps.org/Howto_kappa.html.
[46] Wang R, Qian S, Zhang Z. Investigation of the aggregation morphology of nanoparticle on the thermal conductivity of nanofluid by molecular dynamics simulations. Int J Heat Mass Transf 2018;127:1138–46.
[47] Jin X, Guan H, Wang R, Huang L, Shao C. The most crucial factor on the thermal conductivity of metal-water nanofluids: match degree of the phonon density of state. Powder Technol 2022;412:117969.
[48] Guan H, Su Q, Wang R, Huang L, Shao C, Zhu Z. Why can hybrid nanofluid improve thermal conductivity more? a molecular dynamics simulation. J Mol Liq 2023:121178.
[49] Liu B, Khalid I, Patra I, Kuzichkin OR, Sivaraman R, Jalil AT, Sagban R, Smaisim GF, Majdi HS, Hekmatifar M. The effect of hydrophilic and hydrophobic surfaces on the thermal and atomic behavior of ammonia/copper nanofluid using molecular dynamics simulation. J Mol Liq 2022;364:119925.
[50] Zeng S, Xue R, Sabetvand R. Molecular dynamics study on the effect of external electric field on thermal properties of ammonia/copper nano-refrigerant in a nanochannel equipped with different types of cavities. Int Commun Heat Mass Transfer 2022;130:105802.
[51] Toghraie D, Hekmatifar M, Salehipour Y, Afrand M. Molecular dynamics simulation of Couette and Poiseuille Water-Copper nanofluid flows in rough and smooth nanochannels with different roughness configurations. Chem Phys 2019;527:110505.
[52] Rappé AK, Casewit CJ, Colwell K, Goddard III WA, Skiff WM. UFF, a full periodic table force field for molecular mechanics and molecular dynamics simulations. J. Am. Chem. Soc. 1992;114(25):10024–35.
[53] Mayo SL, Olafson BD, Goddard WA. DREIDING: a generic force field for molecular simulations. J Phys Chem 1990;94(26):8897–909.
[54] https://docs.lammps.org/pair_modify.html.
[55] Huray PG. Maxwell's equations. John Wiley & Sons; 2011.
[56] https://docs.lammps.org/fix_ave_chunk.html.
[57] Mohagheghian S, Elbing BR. Characterization of bubble size distributions within a bubble column. Fluids 2018;3(1):13.
[58] Chen S, Zhang Y, Wang J, Zhao H. Key role of asymmetric interactions in low-dimensional heat transport. J Stat Mech: Theory Exp 2016;2016(3):033205.
[59] Karimi A, Afghahi SSS, Shariatmadar H, Ashjaee M. Experimental investigation on thermal conductivity of MFe2O4 (M= Fe and Co) magnetic nanofluids under influence of magnetic field. Thermochim Acta 2014;598:59–67.
[60] Suh YJ, Cho K. Thermal conductivity enhancement of magnetic fluids under magnetic field based on percolation theory. Mater Trans 2015;56(8):1262–8.
[61] Doganay S, Alsangur R, Turgut A. Effect of external magnetic field on thermal conductivity and viscosity of magnetic nanofluids: a review. Mater Res Express 2019;6(11):112003.
[62] Greenlee H. Motion of a charged particle in a magnetic field. DØ Note 2003;4180.
[63] Xiang Z, Jakkpat K-I, Ducharne B, Capsal J-F, Mogniotte J-F, Lermusiaux P, Cottinet P-J, Schiava NDella, Le MQ. Enhancing the low-frequency induction heating effect of magnetic composites for medical applications. Polymers (Basel) 2020;12(2):386.
[64] Coronel-Escamilla A, Gómez-Aguilar J, Alvarado-Méndez E, Guerrero-Ramírez G, Escobar-Jiménez R. Fractional dynamics of charged particles in magnetic fields. Int J Modern Phys C 2016;27(08):1650084.
[65] Sheikholeslami M, Rokni HB. Simulation of nanofluid heat transfer in presence of magnetic field: a review. Int J Heat Mass Transf 2017;115:1203–33.
[66] Liu X, Ghafari B, Patra I, Kadhim MM, Jalil AT, Kumar TA, Sivaraman R, Nasajpour-Esfahani N, Andani MT, Toghraie D. A molecular dynamics study of thermal behavior of ammonia/Cu nanorefrigerant flow under different initial pressures and electric fields. J Mol Liq 2022;367:120388.
[67] Mlakar G. Effects of surface engineering on HFE-7100 pool boiling heat transfer. Case Western Reserve University; 2021.
[68] Hu H, Xu C, Zhao Y, Ziegler KJ, Chung J. Boiling and quenching heat transfer advancement by nanoscale surface modification. Sci Rep 2017;7(1):1–16.
[69] Du J, Su Q, Li L, Wang R, Zhu Z. Evaluation of the influence of aggregation morphology on thermal conductivity of nanofluid by a new MPCD-MD hybrid method. Int Commun Heat Mass Transfer 2021;127:105501.
[70] Wang R, Zhang Z, Li L, Zhu Z. Preference parameters for the calculation of thermal conductivity by multiparticle collision dynamics. Entropy 2021;23(10):1325.